

Humanoid Whole-Body Badminton via Multi-Stage Reinforcement Learning

Chenhao Liu*, Leyun Jiang[†], Yibo Wang[†], Kairan Yao, Jinchen Fu and Xiaoyu Ren
 Beijing Phybot Technology Co., Ltd, Beijing, China 100089
 Email: liuchenhao@phybot.cn

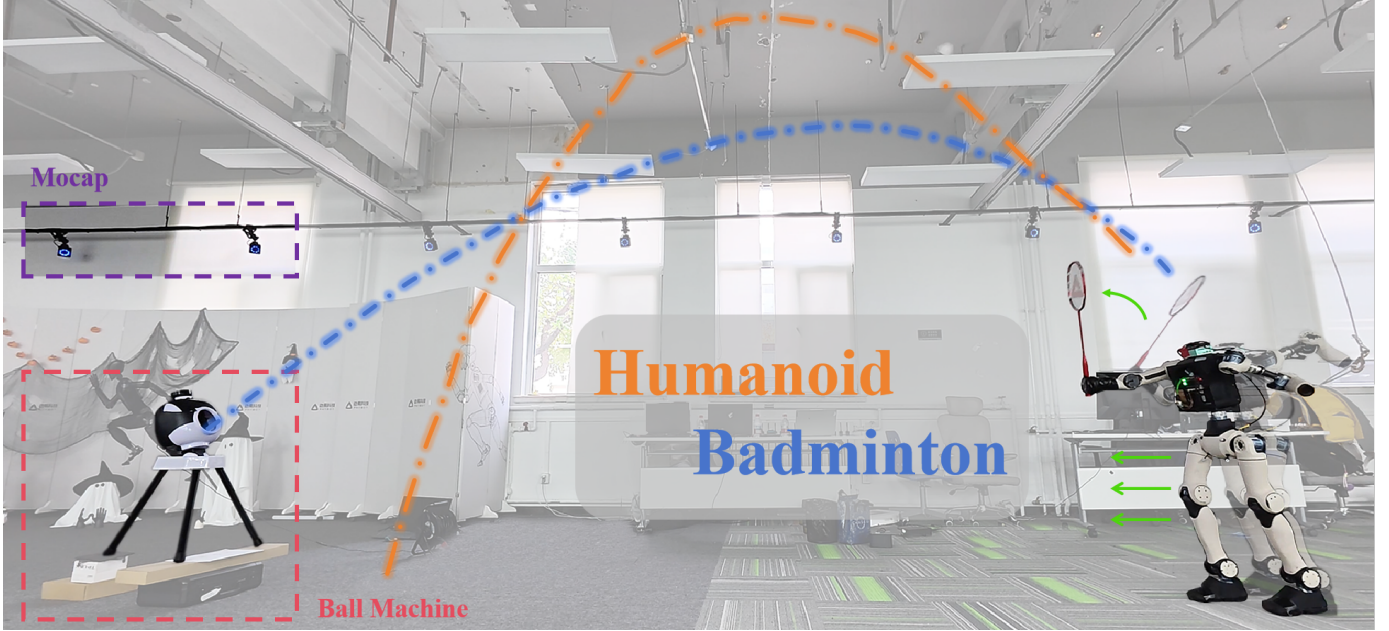


Fig. 1: **Real-world humanoid badminton.** A fully autonomous humanoid returns machine-fed shuttles in a motion-capture arena; overlaid arcs show an incoming (blue) and returned (orange) trajectory. Project Page: humanoid-badminton.github.io.

Abstract—Humanoid robots have demonstrated strong capability for interacting with deterministic scenes across locomotion, manipulation, and more challenging loco-manipulation tasks. Yet the real world is dynamic, quasi-static interactions are insufficient to cope with the various environmental conditions. As a step toward more dynamic interaction scenario, we present a reinforcement-learning-based training pipeline that produces a unified whole-body controller for humanoid badminton, enabling coordinated lower-body footwork and upper-body striking without any motion priors or expert demonstrations. Training follows a three-stage curriculum—first footwork acquisition, then precision-guided racket swing generation, and finally task-focused refinement—yielding motions in which both legs and arms serve the hitting objective. For deployment, we incorporate an Extended Kalman Filter (EKF) to estimate and predict shuttlecock trajectories for target striking. We also introduce a prediction-free variant that dispenses with EKF and explicit trajectory prediction. To validate the framework, we conduct five sets of experiment in both simulation and the real world. In simulation, two robots sustain a rally of 21 consecutive hits. Moreover, the prediction-free variant achieves successful hits with comparable performance relative to the target-known policy. In real-world tests, both the prediction and controller module exhibit high accuracy, and on-court hitting achieves an outgoing shuttle speed up to 10 m/s with a mean return landing distance of 3.5 m. These experiment results show that our humanoid

robot can deliver highly dynamic while precise goal striking in badminton, and can be adapted to more dynamism critical domains.

I. INTRODUCTION

Humanoid platforms have been proposed as general-purpose embodied agents for human-compatible skills [1, 2]. Despite rapid progress in locomotion and motion imitation, agile, contact-rich interactions with fast-moving objects under tight reaction windows remain underexplored. Badminton is a particularly ideal testbed: returns require sub-second perception–action loops, precisely timed and oriented racket–shuttle contacts within a large 3D interception volume, and whole-body coordination that blends rapid arm swings with stable and agile leg motions.

Compared with several recent works on robot table tennis [3, 4, 5], badminton aggravates several difficulties. Aerodynamics are highly uncertain: strong drag and a non-parabolic “flip” regime make the pre-turning trajectory hard to model; as a result, the seemingly longer flight still yields less usable decision time. Although the racket face is larger, valid hits occur only in brief windows when position, velocity, and orientation

align; swing amplitudes are also much larger, injecting angular momentum that challenges whole-body balance. Critically, footwork and striking must co-evolve: lower-body motion does not merely reposition the base but co-determines hitting accuracy. Our system reaches swing speeds around 5.3 m/s and produces outgoing shuttle speeds up to 10 m/s. The serve-to-hit window is 0.8 to 1.0 s; the first 0.36 s is consumed by trajectory prediction, leaving less than 0.6 s for the controller to react.

Humanoids are a natural fit for badminton. Lateral mobility and reach patterns match human-centered rules and court geometry, and established human strategies (e.g., split steps, approach phases, recovery) transfer more directly compared to the non-humanoid platforms. Demonstrating badminton on a humanoid, therefore, serves as a stepping stone toward broader, high-dynamics, and interactive behaviors in human environments.

Related efforts highlight both promise and gaps. [5] demonstrated humanoid table tennis via a hierarchical planner coupled to a learned whole-body controller and achieved long rallies. Our setting differs in key ways: (i) we do not use reference motions to shape striking; instead, the policy discovers energy-efficient swings purely via reinforcement learning, simplifying implementation, and avoiding excessive style constraints; (ii) The use of “virtual hit plane” reduces striking to a largely 2D problem, whereas badminton demands orientation-aware contacts throughout a 3D free space; and (iii) badminton’s large-amplitude strokes induce significant whole-body disturbance, requiring balance recovery that table-tennis-scale motions seldom provoke. Closer to badminton, recent work on legged mobile manipulation learns coordinated skills with onboard vision [6]; however, humanoid hardware deployment remained elusive, and their simulated policies did not exhibit badminton-style footwork, suggesting missing training signals for lower-body coordination. These gaps motivate a training pipeline that explicitly fosters footwork–strike synergy on humanoids and scales to real hardware.

This paper presents, to our knowledge, the first real-world humanoid robot that plays badminton. We train a unified whole-body controller with a multi-stage reinforcement learning curriculum: (1) footwork acquisition toward target regions with feet-swing time and height regularization; (2)precision-guided arm swing generation with timing and scheduled tightening of position and orientation accuracy; and (3) final refinement that removes most locomotion-shaping regularizers to avoid gradient interference and maximize hitting performance. Across all stages, we adopt the shuttlecock simulation of [6] to generate flight trajectories for training. At each rollout, the policy receives a compact target tuple—hit time, intercept position, and racket orientation—drawn from a pre-generated corpus of about 20k trajectories; intercepts are selected randomly within a 1.5–1.6 m height band. Exponential rewards with scheduled tightness transition behavior from coarse to precise.

The policy observes target hit information as well as proprioception and inferred actions for 21 joints on a 1.28 m

custom humanoid. In deployment, the hitting target is obtained online from an EKF that predicts the shuttlecock trajectory. We leverage a Low-level PD controller that runs at 500 Hz, with policy inference at 50 Hz to derive the desired joint position. Training occurs fully in simulation with moderate domain randomization, and the final control policy is deployed in a zero-shot manner without system identification or manual parameter adjustment. We conduct the real-world experiments in a motion capture (Mocap) arena with a serving machine.

Beyond the default pipeline, we also study a prediction-free variant that removes the explicit shuttle-trajectory predictor. During training, the actor only receives instantaneous shuttle pose plus five history pose frames to infer hit timing and pose; the critic retains privileged targets (asymmetric actor–critic) to better learn the value function [7]. This end-to-end control strategy aligns with human intuition (rolling anticipation), simplifies deployment by avoiding predictor or planner retuning, and naturally supports aerodynamic randomization. We report simulation-base comparison results in this work while leave real-robot validation to the future work.

Both simulation and real world results indicate that our humanoid can execute large-amplitude swings while maintaining balance, react within sub-second windows, and intercept fast incoming shuttles fully autonomously without the aid of teleportation or motion demonstrations. While our current tests focus on machine-served shuttles in the Mocap arena, observed behaviors from the training recipe suggest a feasible path to higher-ceiling venues and, ultimately, rallies with robotic or human opponents. The key technical contributions are summarized as follows:

- First real-world humanoid badminton: an autonomous, unified whole-body controller that returns machine-served shuttles on a 21-DoF humanoid, achieving about 5.3 m/s swing speeds and producing outgoing shuttle speeds up to 10 m/s under sub-second reaction.
- Stage-wise RL for footwork–strike coordination: a three-stage curriculum that first establishes footwork, then introduces swing generation and precision striking, and finally removes locomotion-shaping regularizers to maximize hitting performance.
- A prediction-free variant: a more end-to-end policy that infers timing and hitting target implicitly from short-horizon shuttle observations, improving robustness to aerodynamic variability and simplifying deployment by removing EKF-based trajectory predictor.

II. RELATED WORK

A. Mobile Whole-Body Control

Combining manipulation skills with flexible mobile ability is essential for a wide range of robotic applications. Typically, the base movement and end-effector tracking problems can be solved separately to reduce task complexity [8, 9]. The work in [9] proposes an MPC controller to track the desired end-effector position of an arm mounted on the quadruped with a standalone RL-based controller for locomotion. To catch objects in flight, [10] assigns the base movement, arm swing,

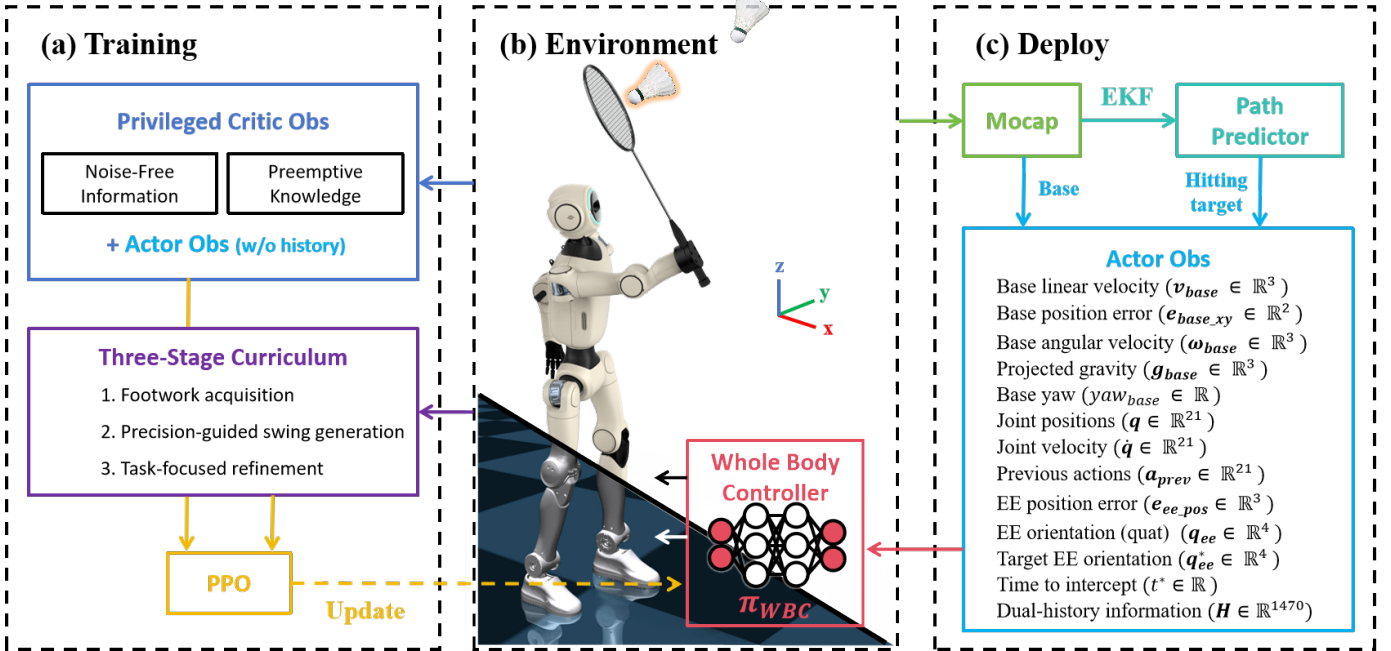


Fig. 2: **System overview.** (a) **Training:** PPO learns a single policy π_{WBC} using Privileged Critic Obs (Noise-Free Information, Preemptive Knowledge) and Actor Obs (no history) under a three-stage curriculum. All observations and rewards in (a) come from the simulation environment. (b) **Environment:** The humanoid is 1.28 m tall, weighs 30 kg, and has 21 DoF. A 3D-printed mount attaches the racket orthogonally to the forearm. The robot is initialized above the origin and faces the $+x$ direction. Shuttlecock position and base pose are obtained by motion capture using the marker. (c) **Deploy:** At runtime, Mocap directly provides the base state, while an EKF with a path predictor estimates the shuttle trajectory to produce the hitting target $\{p_{ee}^*, q_{ee}^*, t^*\}$. This information, together with proprioception and dual-history features, forms the complete Actor Obs. π_{WBC} consumes the Actor Obs and outputs whole-body actions executed by a low-level PD controller.

and hand catching tasks to three policy modules. Similarly, [8] claims that decoupling upper-body and lower-body control into separate agents can achieve a more precise end-effector tacking performance when the robot is moving.

Despite these promising advantages, there are still many efforts made to unify the lower and upper body control [11, 12, 13]. Specifically, [11, 12], [14] leverage a multi-critic architecture to ease the optimization of the coordinated behavior. Moreover, [13] introduces a physical feasibility reward design to guide the unified policy learning. As for recent works on dynamic whole-body tasks such as racket sports and tossing, performance hinges on coordinated whole-body impulse generation and timing, with the legs contributing to power transmission rather than merely locomotion. Unified whole-body control has proved effective across these domains [15], [6], [16].

B. Robotic Racket Sports

Devising control strategies for robotic Racket Sports has been a fundamental research benchmark that helps inspect progress on the whole-body control algorithms [5, 3, 17, 6]. The intensive coupling of environmental perception, target

reaching, and precise end-effector control brings a critical challenge to the system design. To achieve an amateur human-level table tennis competition, [3] introduces a hierarchical and modular policy architecture to handle the unseen scenarios when playing with human. Despite the impressive result in [3], [5] shows that a reinforcement learning-based whole-body controller with a simple model-based planner for ball trajectory prediction and racket target planning are competent for a humanoid robot to conduct consecutive shots with a human opponent. More recently, [6] introduces a perception-informed whole-body visuomotor policy that achieves effective shuttlecock tracking and striking using a quadrupedal platform for the badminton task. However, we assume that the humanoid robot platform shows a more consistent motion pattern with humans for the badminton task. In this work, we focus on the coordinated badminton skill learning on a self-developed humanoid platform and conduct a systematic evaluation of the controller’s performance.

III. SYSTEM OVERVIEW

Platform. Our robot is a self-developed general-purpose humanoid Phybot C1 (1.28 m, 30 kg, 21 DoF), see Fig. 2 (b).

DoF distribution: each leg has 3 hip joints, 1 knee, 2 ankle; the torso has 1 waist; each arm has 3 shoulder joints and 1 elbow. All joints use cycloidal-reduction actuators. Lower-body peak torques span 96–244 Nm; most arm joints are 96 Nm except shoulder-yaw (12 Nm). Motors reach maximum 15 rad/s. A standard 100 g full size badminton racket is rigidly clamped to the distal forearm by a 3D-printed mount, with the racket perpendicular to the forearm axis. Onboard sensing comprises an IMU and absolute encoders; we do not employ force or tactile sensors.

Environment and frames. Experiments are conducted in a Mocap arena. The world frame is fixed to the court floor; to remain consistent with training, the robot is initialized nearly above the world origin and faces the positive x direction; z is upward. The mocap optical volume loses the shuttle above 2.8 m, so all serves are preferably constrained below this height.

Perception. A FZMotion motion capture system with 21 cameras provides measurements streamed over Wi-Fi to the robot. Markers are placed on the robot base, yielding base position, orientation, and linear velocity; the shuttle carries reflective tape on the tip and provides position only (insufficient features to instantiate a rigid body). Our nominal pipeline estimates shuttle state via an EKF and predicts interception by forward dynamics integration. A prediction-free variant bypasses forecasting and feeds only the current and a short history of shuttle positions to the policy.

Compute, control, and communications. All inference and control run on an Allspark-2 x86 platform with an Intel Core i7-1165G7. The onboard computer communicates with the motor control board via wired CAN (command path < 1 ms), and the control board drives all actuators on a CAN bus. Mocap data arrive over a Wi-Fi router, with typical delays of tens of milliseconds (about 1–2 policy cycles depending on link stability). Frequencies: mocap 210 Hz; policy 50 Hz; low-level PD controller 500 Hz. Per-joint PD gains and actuator constants are listed in the appendix.

External devices and power. Serves are produced by a manually aimed ball machine with adjustable position and launching angle, up to 14 m/s shuttle speed. The robot is powered by a 72 V battery pack. Further hardware specifications (joint limits, torque constants, detailed parameters) are provided in the appendix.

IV. LEARNING COORDINATED BADMINTON POLICY

A. RL-based Dynamic Whole-Body Controller

1) Multi-Stage Reinforcement Learning: We cast policy learning as a partially observable Markov Decision Process (MDP) $\mathcal{M} = (\mathcal{S}, \mathcal{O}, \mathcal{A}, \mathcal{P}, \mathcal{R})$. At time t , the (unobserved) state is $s_t \in \mathcal{S}$; the agent receives an observation $o_t \in \mathcal{O}$, applies action $a_t \in \mathcal{A}$, transitions with $s_{t+1} \sim \mathcal{P}(\cdot | s_t, a_t)$, and accrues reward $r_t = \mathcal{R}(s_t, a_t)$. We learn a parametric policy $\pi_\theta(a_t | o_t)$ that maximizes $J(\theta) = \mathbb{E}[\sum_t \gamma^t r_t]$.

Observation space. The actor’s basic observation is 87-D, concatenating proprioception information and external sensing from Mocap. On top of this 87-D vector, we stack short/long history of all joint positions, velocities, and actions (5 frames +

20 frames) [18], adding up to 1,557 features to mitigate partial observability (e.g., base-velocity noise). The critic observation has 98 dimensions in total, which include the privileged information used to enhance actor version observations, such as noise-free base and joint states as well as racket speed which may be difficult to acquire in the real world. Others are classified as preemptive knowledge used to make MDP well-posed for accurate value learning. All quantities are expressed in the world frame. Detailed information are listed in Fig. 2(a), (c).

Action space. The policy outputs 21 joint position targets for all DoF, scaled by a unified action scale of 0.25 and tracked by the low-level PD controller.

Episodes Settings. Each episode contains six swing targets, following the configuration used by [6]. This design enables follow-through behavior learning but makes the value function depend on the number of hits remaining. We therefore adopt an asymmetric actor–critic [19] the critic receives additional preemptive information as mentioned above to stabilize value estimation, while the actor only uses deployable observations. Concretely, these are two subsequent hitting times, next target position and orientation, and the number of remaining targets.

Training Settings. We train with PPO [20] on a single Nvidia RTX 4090 using 4096 parallel environments in IsaacGym [21]. Both actor and critic are MLPs with hidden layers 512–256–128 and ELU activations. Other hyperparameters are reported in the appendix.

Three-stage curriculum. As shown in Fig. 2(a), we use a three-stage schedule with identical observation and action space across stages; only reward terms and their weights change. Training in each stage continues from the previous checkpoint once each stage’s primary objective has converged. The whole process throughout all stages takes 12.4 h wall-clock time on a single RTX 4090, after which the policy is ready for deployment.

- S1 — Footwork acquisition toward sampled hit regions: learn to approach target regions with reasonable lower limb gait and maintain a stable, forward-facing posture while traversing between six sampled hit locations within an episode.
- S2 — Precision-guided swing generation: building on S1, introduce a sparse hit reward active only at the scheduled hit instant t^* to enforce timing. Start with loose pose accuracy to let a full swing emerge, then schedule tightening of position and orientation accuracy. Add light swing-style regularization for human-like kinematics, and strengthen energy, torque, and collision constraints for efficient, stable hits.
- S3 — Task-focused refinement: remove target approach rewards (which is the main task reward in S1) and most gait-shaping regularization (e.g. foot distance, step/contact symmetry, step height) to avoid gradient interference with the hitting objective; keep safety, energy, hardware limit constraint terms. Domain randomization and observation noise are enabled here to consolidate robustness.

We conduct a simple ablation study. Removing S1 and starting from S2 causes training to diverge directly. Using S1–S2 yields a hardware-deployable policy but there’s still room for improvement. S3 breaks this plateau and improves performance and robustness.

2) *Multi-Stage Reward Design*: We devise a modular reward function that consists of a locomotion-style term r_{loco} and an arm hitting term r_{hit} to guide the emergence of coordinated badminton skills. The locomotion reward follows [22] and leverages feet swing-time to encode step frequency implicitly. While the hit reward references [6] but making some modifications. We group the remaining terms into global regularization (action rate, joint limits, collision, energy etc.). Exact weights are reported in the appendix.

S1 — Footwork acquisition. Let $d = \|(p_{\text{ee}}^* - p_{\text{base}})_{xy}\|$. The main shaping encourages reaching the target region while not necessarily requiring precise approach, being nearby will suffice:

$$r_{\text{track}} = \exp(-4 \max(d - 0.3, 0)). \quad (1)$$

S1 applies standard style shaping for humanoid stable walking—base height and orientation, acceleration regularization, contact-aware footstep terms (air time, touchdown speed, step height, foot posture, no-double-flight), and simple gait symmetry shaping—plus face alignment to the incoming shuttle. Safety constraints (action rate, joint position/velocity/acceleration, torque, energy) follow legged_gym conventions [22]. With this shaping, S1 typically converges within 1k iterations, yielding reliable target-region tracking with natural gait.

S2 — Precision-guided swing generation. On top of S1, we lower the weight of regional tracking and introduce a hit-instant reward with large weight (six activations per episode). This reward comes with two terms, hitting precision and racket swinging speed. While [6] splits hitting precision into position and orientation with different scale, we find it to be more accurate to entangle two terms together, coupling position and orientation accuracy [15]. Then we introduce another racket speed term to encourage swing. Define the target racket normal n^* as the negative z -axis of target hitting orientation q_{ee}^* . Let v_{ee} be the end-effector linear velocity; the effective speed component in the direction of target is $v_{\text{ee}} \cdot n^*$ (clamped at ≥ 0). Let $e_{\text{ee_pos}} = \|p_{\text{ee}} - p_{\text{ee}}^*\|$ and $e_{\text{ee_ori}} = \text{ang_err}_z(q_{\text{ee}}, q_{\text{ee}}^*)$. The hit reward, active only at $t = t^*$, is

$$\begin{cases} r_{\text{swing}} = \exp\left(-\frac{e_{\text{ee_pos}}^2}{\sigma_p}\right) \exp\left(-\frac{e_{\text{ee_ori}}}{\sigma_r}\right) + 0.3 r_v, \\ r_v = 1 - \exp\left(-\frac{\max(0, v_{\text{ee}} \cdot n^*)}{\sigma_v}\right). \end{cases} \quad (2)$$

We start with wide pose tolerances $\sigma_p = 2.0$, $\sigma_r = 8.0$ to allow a full swing to emerge, and then schedule tightening of position and orientation accuracy to $\sigma_p = 0.1$, $\sigma_r = 1.0$ as training progresses. The racket speed sigma is fixed at $\sigma_v = 3.0$, so a 5 m/s swing yields $> 80\%$ of the speed term, balancing accuracy with deploy-time stability. We also add light swing-style regularization to align the racket short-

edge (y) axis with the world y -axis,

$$r_{\text{y-align}} = (\hat{\mathbf{y}}_{\text{ee}}^\top \hat{\mathbf{y}}_{\text{world}})^2, \quad \hat{\mathbf{y}}_{\text{ee}} = R(q_{\text{ee}}) \mathbf{e}_y, \quad (3)$$

which encourages the policy to adopt a more human-like hitting posture—performing a backswing and then swinging forward along the reverse of that backswing—to produce a more complete kinetic chain. And reward a default holding pose when no shuttle is launched,

$$r_{\text{hold}} = - \sum_{j \in \mathcal{A}_{\text{arm}}} (q_j - q_j^{\text{hold}})^2, \quad (4)$$

where \mathcal{A}_{arm} denotes the set of arm joint indices. This improves deploy-time stability and recoverability. We also add collision penalties and strengthen energy, torque costs. In practice, policy first learns to bring the racket near the target and gradually develops an early backswing then swing with peak velocity near t^* ; with the scheduled tightening, after about 20k iterations, it progress to smooth backswing–swing–recovery with practical precision.

S3 — Task-focused refinement. Starting from the S2 checkpoint, we remove most gait-shaping terms in r_{loco} —foot distance, contact and step symmetry, optimal footholds, step height—to avoid gradient conflict with the hitting objective. We retain gloable regularization terms and r_{hit} rewards, and enable domain randomization plus observation noise to consolidate robustness. With these enabled—thus making the environment deliberately harder—the policy does not regress; instead, we observe consistent improvements across metrics. The primary hitting reward r_{swing} increases by 3–5%, and we see lower action rates, reduced joint velocity and acceleration penalties, lower energy consumption, cleaner foot-contact force profiles, and reduced joint-torque usage; notably, the energy and torque costs decrease by $\approx 20\%$ empirically.

Global regularization (all stages). Action rate penalties, joint position/velocity/acceleration, torque limits follow standard legged gym practice; thresholds and weights are listed in the appendix.

B. Model-based Hitting Target Generation and Prediction

Building on the work presented in [6], we similarly adopted a model-based approach for both generating shuttlecock trajectories required for robot training and predicting hitting positions using physical models.

1) *Generate Shuttlecock Trajectory for Training*: To generate badminton flight trajectories for training purposes, we employed a physics-based simulation approach. This method adheres to the badminton dynamics model in [23], with the shuttlecock’s flight state updated according to the following equation:

$$m \frac{dv}{dt} = mg - m \frac{\|\mathbf{v}\| \mathbf{v}}{L} \quad (5)$$

where m represents the shuttlecock mass, v denotes its velocity, g is gravitational acceleration, and L is the aerodynamic length, defined as $L = 2m/\rho S C_D$. Here, ρ is air density, S is the cross-sectional area of the shuttlecock, and C_D is the

drag coefficient. The computed aerodynamic length L used in our work is 3.4.

The generated shuttlecock flight trajectories were required to meet specific conditions to ensure data validity and relevance. To simulate realistic badminton hitting scenarios, we defined a hitting zone constrained by $x \in [-0.8, 0.8]$, $y \in [-1, 0.2]$, and $z \in [1.5, 1.6]$, with a minimum traversal time of 0.8 seconds. This filtering process effectively eliminated trajectories that did not conform to realistic hitting requirements, thereby ensuring the quality of the training data. Hitting zone on y direction is unsymmetrical due to right hand racket setting.

Finally, the selected trajectories were combined with corresponding traversal point data to construct a comprehensive training dataset containing position, orientation (tangential line of the trajectory) and timing features. These data are stored as tensors and can be directly utilized for subsequent training.

2) *Shuttlecock Trajectory Prediction for Deployment*: In the deployment phase, an EKF-based trajectory prediction algorithm was developed to achieve real-time shuttlecock flight estimation and hitting point prediction. This approach accounts for aerodynamic drag, gravitational acceleration, and sensor noise, providing accurate target for the robot's striking motion planning.

Our Extended Kalman Filter implementation adheres to the same badminton dynamics model as that used for shuttlecock trajectory generation. The system state vector is defined as:

$$\mathbf{x} = [x, y, z, v_x, v_y, v_z]^\top \quad (6)$$

where position $[x, y, z]$ and velocity $[v_x, v_y, v_z]$ are expressed in the global coordinate frame.

The Extended Kalman Filter operates through two distinct phases: measurement update and prediction. When the predicted height first falls below the predefined hitting plane at $z = z_{target}$, linear interpolation is employed to compute the spatial coordinates and time of traversal. This calculated point is designated as the predicted hitting point, with its position and time expressed as: $\mathbf{p}_{ee}^* = [x_{hit}, y_{hit}, z_{target}]^\top$ and t^* .

The corresponding velocity vector at t_{hit} is then converted into a quaternion representation to guide the robot's end-effector orientation during the hitting motion.

C. Prediction-free variant

We additionally train a prediction-free policy whose only change from the main pipeline lies in the observation space; the reward function, action space, training schedule (three-stage) remain identical. In this variant, the actor no longer receives the commanded hitting position, orientation and time $(p_{ee}^*, q_{ee}^*, t^*)$. Instead, it ingests a sliding window of world-frame shuttle positions comprising the current frame and the previous five frames sampled at 50 Hz (i.e., $\{p_{sh}(t), p_{sh}(t-0.02), \dots, p_{sh}(t-0.10)\}$). From this short history the actor must implicitly infer the intended interception pose and timing. The critic retains privileged access to the "actual" interception point. This design is enabled by how training data are generated: for each commanded target, we

do not only sample the single interception point but also store the entire shuttle trajectory integrated by forward badminton dynamics. During training, the reward and the critic always know the ground-truth hit specification associated with the current shot, while the actor only observes the raw shuttle-history window.

A practical advantage is that deployment no longer requires a hand-tuned predictor (e.g., EKF plus aerodynamic model) to deliver $(p_{ee}^*, q_{ee}^*, t^*)$. Instead, the controller conditions on directly measured shuttle positions, greatly reducing sensitivity to mismatches in physical or estimator parameters. To further improve robustness, we randomize aerodynamic parameters per shot, effectively treating the simulator as having an "aerodynamic patch" whose exact coefficients need not be identified. Intuitively, this mirrors human play: players do not know a specific shuttle's drag constants a priori but can infer landing tendencies from a brief flight segment. In simulation we observe that the prediction-free policy achieves hitting with a small performance drop relative to the known-target setting, while simplifying deployment by removing the need to retune predictor and physics parameters. Real-robot validation of this variant is left to future work.

V. EXPERIMENTS

We evaluate our approach with five experiments that together probe accuracy, agility, robustness, and deployability: (1) a simulation **Two-Robot Rally** that measures sustained rally length; (2) a simulation **Target-Known vs. Prediction-Free Comparison** that contrasts two observation designs under matched conditions; (3) an **EKF Prediction Accuracy** study that quantifies trajectory and intercept-point errors; (4) a real-world **Virtual-Target Swinging** test that assesses swing speed and pose accuracy without a real shuttle; and (5) a real-world **Ball-Machine Hitting** test that measures outgoing shuttle speed, reachable interception range, and return landing distribution.

A. Experiment Settings

All simulation studies are performed in Isaac Gym and MuJoCo. Isaac Gym runs on a single RTX 4090; MuJoCo runs on CPU. During testing, a policy may hit any number of shuttles within an episode, not limited to six as training. For on-robot feasibility, we adopt a design target for "hit success" of position error below 0.10 m and orientation error below 0.2 rad at the scheduled impact time. This target is motivated by the racket geometry: 0.10 m is approximately the half-width of the racket's short axis. In simulation, the controller's ability to meet or exceed this target is what makes real-world hits possible later.

For simulation, the Two-Robot Rally uses a scaled singles court tailored to a 1.28 m humanoid: half-court length 4.0 m along x , half-court width 1.75 m along y , and a net height of 1.524 m. Unless otherwise noted, the aerodynamic model matches the one used to generate training trajectories. When evaluating the Prediction-Free policy we also vary the aerodynamic characteristic length within a bounded range to emulate

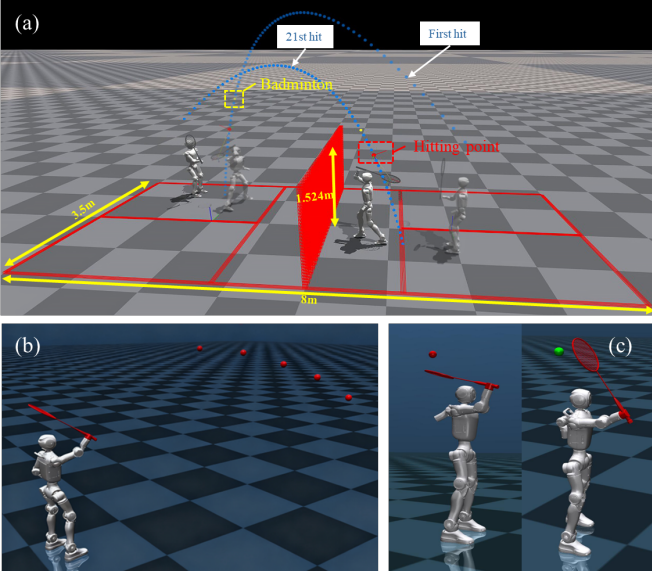


Fig. 3: **Simulation.** Figure (a) illustrates the Two-Robot Rally scenario, where two identical humanoid robots sustain a rally of 21 consecutive returns. Figure (b) demonstrates the Prediction-Free policy: the robot infers the optimal impact position and orientation solely from the first five recorded shuttlecock positions after serving. Figure (c) presents the Target-Known policy, where a predetermined hitting position is provided. The red sphere indicates the designated hitting location, while the green sphere confirms successful impact execution by the robot.

different shuttles, while the Target-Known policy uses the fixed aerodynamics from training. For hardware deployment, the robot operates in a Mocap arena. The ball machine is placed at approximately $x = 5.2$ m from the origin. Interception heights are kept within 1.5–1.6 m to match training. The Virtual-Target Swinging test commands spatial targets without a shuttle to isolate swing behavior. The Ball-Machine Hitting test narrows the interception region for safety and field-of-view reasons and measures interception area and returns.

B. Simulation Results

1) *Two-Robot Rally:* Two identical humanoids stand on opposite sides of the scaled court, see Fig. 3 (a), both right-handed and both running the same Target-Known policy. The first interception target is sampled from the training-style distribution. After a side attempts a hit, we compute the outgoing shuttle velocity from the incoming shuttle state and the racket state at the contact instant, assuming a nearly elastic interaction with a racket inertia that dominates the shuttle. With racket-face normal n_{racket} , incoming velocity v_{incoming} , and racket velocity v_{racket} , we have:

$$\begin{cases} v_{\text{racket},n} = (v_{\text{racket}} \cdot n_{\text{racket}}) n_{\text{racket}}, \\ v_{\text{shuttle},n} = (v_{\text{incoming}} \cdot n_{\text{racket}}) n_{\text{racket}}, \\ v_{\text{out}} = v_{\text{incoming}} - 2v_{\text{shuttle},n} + 2v_{\text{racket},n}. \end{cases} \quad (7)$$

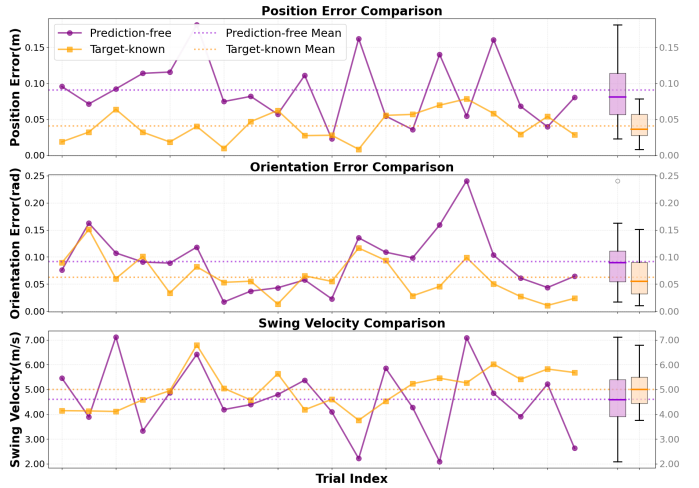


Fig. 4: **Policy comparison.** The top part of this figure shows the **position error** for both strategies. The middle section of the figure shows the **orientation error** comparison, the orientation corresponds to the normal direction of the racket face. The bottom part of the figure compares **swing velocity**.

We then integrate the shuttle dynamics forward until it lands on the opposite half-court and alternate sides. The rally ends if a side falls, if the shuttle does not clear the net, if it lands out of bounds, or when the shuttle contacts the ground after a failed interception. Under this rule, we obtain rallies sustained to 21 consecutive returns, indicating that the controller can repeatedly reposition, return shuttle with high quality, and recover posture across extended exchanges.

2) *Target-Known vs. Prediction-Free Comparison:* This experiment contrasts two observation designs under identical scenes, robot initializations, and court geometry, as demonstrated in Fig. 3 (b) (c). The Target-Known policy receives the planned interception position, orientation, and time. The Prediction-Free policy instead observes the current shuttle position together with a five-frame history at 50 Hz and must infer the impact pose and timing from this short temporal window. All other components, including the reward design and training curriculum, are identical. The Target-Known evaluation uses the fixed aerodynamic parameters from training. The Prediction-Free evaluation samples moderate variations of the aerodynamic characteristic length to emulate different shuttles.

Each policy executes twenty hits sampled randomly. We report two quantities: the position and orientation errors at impact and the executed swing speed. As shown in Fig. 4, explicit target information is not indispensable, the policy can infer both the hitting target and the timing on its own with very small performance drop.

C. Sim2Real Transfer

We train the controller entirely in simulation and deploy to hardware in a zero-shot manner. To improve transfer, we apply domain randomization and observation noise during training; detailed ranges are provided in the appendix. We do

not model additional delays, and we do not fit actuator network model [24] or conduct system identification [25]. Rotor inertias are computed from gear reduction. In practice, the learned controller carries over to the real robot in Mocap arena without special tricks, which we substantiate in the EKF Prediction Accuracy study and the two hardware experiments presented later.

D. Real Robot Deployment

In our real world evaluation, we decompose the shuttlecock hitting task into two prerequisites, trajectory prediction and swing execution, followed by a final integrative test.

1) *EKF Prediction Accuracy study*: Prediction error refers to the deviation between the model’s predicted shuttlecock trajectory and the actual measured trajectory. Accurate trajectory prediction is critical for the robot to hit the shuttlecock at the right time and position. To quantify prediction errors, we collected 20 authentic badminton flight trajectories using a motion capture system. Partial segments of these trajectories were used as measurement input for the EKF. The EKF was then employed to generate predictions, which were subsequently compared against the ground-truth contact positions and timing. The comparative results are presented in Fig. 5. At 0.6 s before impact, the mean predicted position error falls below 100 mm, with the error bound sharply converging over time. By 0.3 s prior to contact, the mean position error has narrowed to 10 mm. Meanwhile, interception timing prediction achieves a mean error of approximately 20 ms at 0.6 s before hitting—already meeting task requirement—and similarly exhibits rapid convergence.

2) *Virtual-Target Swinging*: The racket swing error refers to the spatial deviation between the racket’s contact point with the shuttlecock and the sweet spot during execution. To quantify the robot swing error, massive randomly sampled target position was designated, and Mocap was employed to measure the center position of the racket face. The robot was subsequently instructed to execute the hitting motion, and the actual measured interception point was compared against the commanded target position, the corresponding results are presented in Fig. 6.

We conducted a total of 71 virtual target swinging tests. The results showed a mean Euclidean distance error of 24.29 mm with an average racket speed of 5.32 m/s at impact. These results verify that the robot can effectively control the contact point within the radius of the racket face during complex hitting tasks, confirming its practical feasibility for performing high-precision swinging actions.

3) *Real-World Shuttle Hitting*: When integrating two systems together in the real world, we set a ball machine to serve the shuttlecock, adjust its’ strength and pitch-yaw angle, to examine the capability of the policy. Due to the shuttle’s flat slope being limited in indoor Mocap environment, which left a very short window to react, we constraint the interception area in a reasonable range. We collect 25 hitting results; except for one hitting on the edge of racket frame, the robot all achieves successful shuttle return with coordinated and agile motion. As

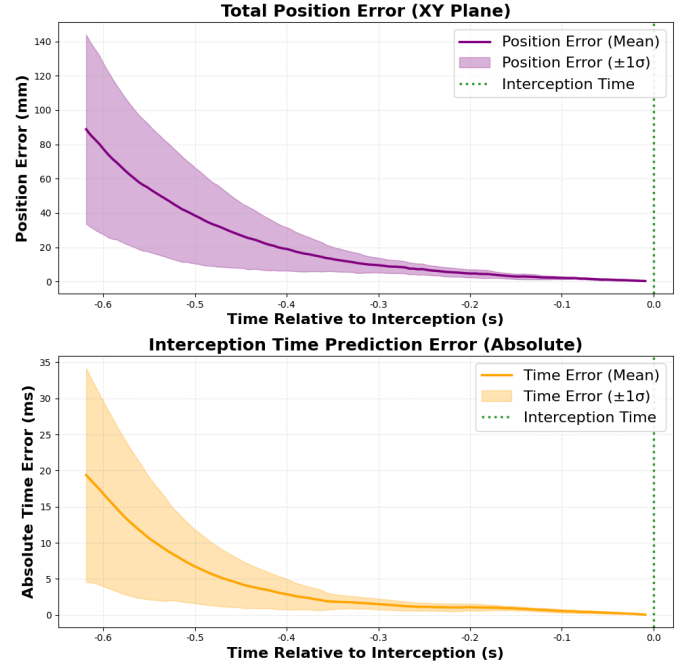


Fig. 5: **EKF Prediction Accuracy**. The predicted striking position error (top) and striking time error (bottom) were evaluated over 20 shuttlecock trajectories. The shaded regions represent the standard deviation. At 0.6 s before interception, the mean position error was less than 100 mm, already smaller than the radius of the racket.

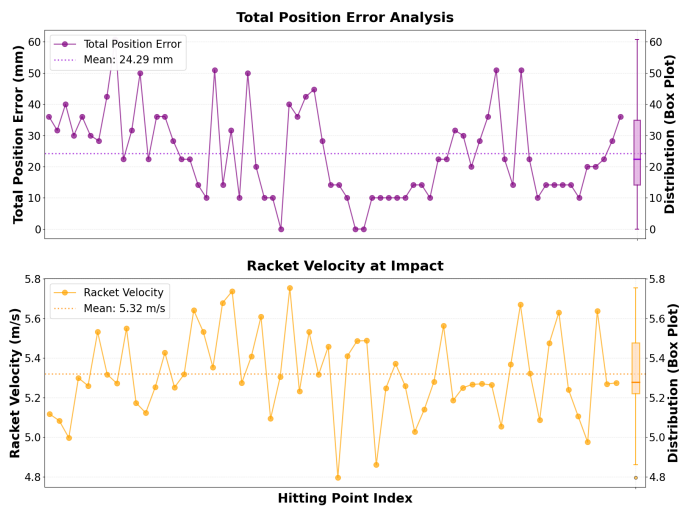


Fig. 6: **Virtual-Target Swinging**. The upper portion of the figure depicts the Euclidean distance error between the racket center and the designated hitting position at the moment of impact, while the lower portion illustrates the corresponding racket speed at impact.

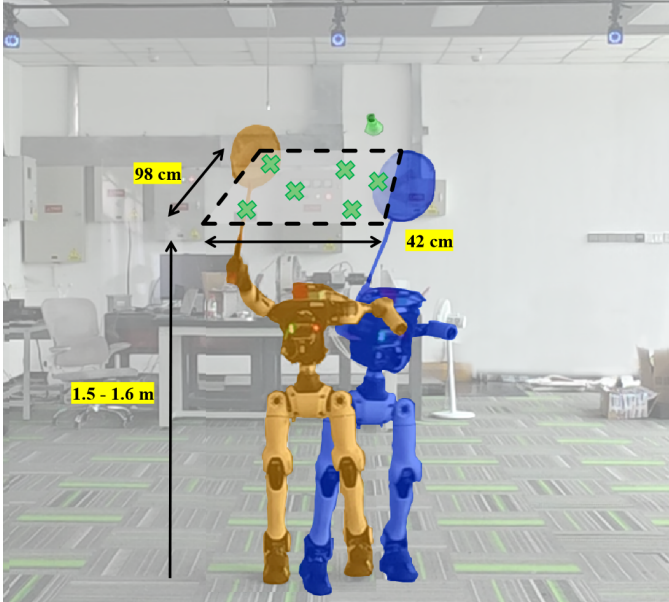


Fig. 7: **Real-World Shuttle Hitting.** This figure captures the robot’s actual hitting postures at the two opposing boundaries of the 98 cm \times 42 cm interception area.

shown in Fig. 7, the robot intercepts the shuttlecock above the ground at about 1.5 m with the range of 98 cm \times 42 cm. This is a relatively large area for a robot height only 1.28 m. We also observe that the robot not only manage to intercept the ball but also return it with high quality, resulting in a sharp slope demonstrated in Fig. 1, with the highest trajectory point over 3 m. Moreover, we measure the return shot landing distance, except for 3 times hitting the ceiling and 1 time hitting on the racket edge it achieves 3.5 m on average away from the interception area.

VI. DISCUSSION

A. System Design

We train a single whole-body policy that coordinates stepping and striking rather than layering an arm controller on top of a lower-body controller. In badminton, hit quality depends on how the legs reposition and supports the arm’s exertion while maintaining balance. The subtle movements of the lower limbs can effectively adjust the posture of the racket.

Our multi-stage curriculum proceeds in three clear steps: learn to reach interception regions with stable footwork; add a sparse, high-value hit signal so a full swing emerges and follow a sigma curriculum to improve accuracy with light style terms; finally remove most lower-limb regularizers to avoid gradients fighting the true objective of precise, energy-efficient hitting. After this removal, hitting metrics continue to improve while energy and torque costs drop, indicating progress toward task-optimal objective. Coupling position and orientation in the hit reward further prevents the policy from over-optimizing one at the expense of the other.

The controller develops two complementary coordination patterns. When the target is nearby or the time budget is

sufficient, it takes short corrective steps and then commits to a backswing. When the target is far or the window is tight, it initiates a long stride while beginning the backswing in parallel. This foot-racket co-timing is not hand-coded; it emerges from the training. Several additional behaviors emerged without explicit incentives. At higher interception heights the policy sometimes produced brief “tiptoe” reaching, and between hits it re-centers near the middle-right of the court, reflecting the sampled target distribution and matching human re-centering behavior.

Using six targets per episode teaches recovery and preparation between hits and reduces dependence on a particular initial posture. The asymmetric actor-critic design also matters: the critic receives preemptive knowledge that makes MDP well-posed and stabilizes value estimation, while the actor is restricted to deployable inputs.

Zero-shot transfer worked because domain randomization covered key dynamics and sensing variations, constraint terms discouraged brittle high-torque solutions, and the staged curriculum encouraged a complete kinetic chain for hitting rather than single-joint-dominant motion.

B. Limitations and Future Work

Dependence on the Mocap arena with limited ceiling height constrains shuttle trajectories to lower arcs driven by a ball machine. During testing, the shuttle occasionally hit the ceiling, and the limited flight range makes long multi-ball rallies with human partners difficult. Higher ceilings and broader interception bands should reveal more of the controller’s potential.

We plan to deploy the prediction-free variant on hardware. It removes explicit target prediction at test time but requires a strictly timed 50 Hz history of shuttle positions. We will add robust buffering and time-stamping so the actor can infer velocities and timing from consistent spacings.

Moving toward pure vision will require reliable visual odometry and policies that keep the shuttle within FOV during aggressive motion. A head-mounted camera that actively tracks the shuttle, together with learning signals that encourage aligning the view with the shuttle trajectory, offers a practical path to remove external tracking.

Above the low-level controller, we will train a higher-level policy by self-play to decide where to intercept, when to swing, and what racket-face orientation to command, then invoke the whole-body controller as a motor primitive. Current failures arise when consecutive targets are too far apart for the available maneuver time. We will address this with wider target sampling and reward shaping that explicitly encourages high-speed legged maneuvers.

Finally, this framework provides a promising path to adapt the pipeline to tennis or squash by replacing the shuttlecock dynamic “patch” and adjusting interception style, with modest reward retuning to reflect different sport-specific behaviors.

VII. CONCLUSIONS

In this work, we present the first real-world humanoid badminton system powered by a unified whole-body RL

policy trained with a three-stage curriculum. The curriculum progresses from guiding lower-body footwork, to inducing a full swing and gradually tightening positional and orientational accuracy, and finally removing most gait regularizers to focus learning on precise, robust hitting. The policy produces human-like badminton behaviors that coordinate stepping and swinging under tight time windows, without any expert demonstrations.

In simulation, two identical humanoids sustain rallies with a best run of 21 consecutive returns, achieving a hitting accuracy within 0.10 m position error and 0.2 rad orientation error. A separate comparison shows that the prediction-free variant matches the counterpart behavior that uses known hitting targets, while remaining robust to moderate aerodynamic variation. On hardware, the controller achieves swing speeds of about 5.3 m/s and returns ball-machine serves with outgoing shuttle speeds up to 10 m/s under sub-second timing, transferring zero-shot through domain randomization. We believe this framework marks an important step toward agile, interactive whole-body response tasks on humanoids. As next steps, we plan to deploy the prediction-free policy on hardware, move toward egocentric vision operation, and layer strategy learning via self-play so the robot can make its own hitting decisions.

REFERENCES

- [1] Ri-Zhao Qiu, Shiqi Yang, Xuxin Cheng, Chaitanya Chawla, Jialong Li, Tairan He, Ge Yan, David J Yoon, Ryan Hoque, Lars Paulsen, et al. Humanoid policy~human policy. *arXiv preprint arXiv:2503.13441*, 2025.
- [2] Tairan He, Zhengyi Luo, Wenli Xiao, Chong Zhang, Kris Kitani, Changliu Liu, and Guanya Shi. Learning human-to-humanoid real-time whole-body teleoperation. In *2024 IEEE/RSJ International Conference on Intelligent Robots and Systems (IROS)*, pages 8944–8951. IEEE, 2024.
- [3] David B DAmbrosio, Saminda Abeyruwan, Laura Graesser, Atil Iscen, Heni Ben Amor, Alex Bewley, Barney J Reed, Krista Reymann, Leila Takayama, Yuval Tassa, et al. Achieving human level competitive robot table tennis. In *2025 IEEE International Conference on Robotics and Automation (ICRA)*, pages 74–82. IEEE, 2025.
- [4] David B D'Ambrosio, Navdeep Jaitly, Vikas Sindhwani, Ken Oslund, Peng Xu, Nevena Lazic, Anish Shankar, Tianli Ding, Jonathan Abelian, Erwin Coumans, et al. Robotic table tennis: A case study into a high speed learning system. In *Robotics: Science and Systems*, 2023.
- [5] Zhi Su, Bike Zhang, Nima Rahamanian, Yuman Gao, Qiayuan Liao, Caitlin Regan, Koushil Sreenath, and S Shankar Sastry. Hitter: A humanoid table tennis robot via hierarchical planning and learning. *arXiv preprint arXiv:2508.21043*, 2025.
- [6] Yuntao Ma, Andrei Cramariuc, Farbod Farshidian, and Marco Hutter. Learning coordinated badminton skills for legged manipulators. *Science Robotics*, 10(102):eadu3922, 2025.
- [7] Lerrel Pinto, Marcin Andrychowicz, Peter Welinder, Wojciech Zaremba, and Pieter Abbeel. Asymmetric actor critic for image-based robot learning. In *Proceedings of Robotics: Science and Systems*, Pittsburgh, Pennsylvania, June 2018.
- [8] Yitang Li, Yuanhang Zhang, Wenli Xiao, Chaoyi Pan, Haoyang Weng, Guanqi He, Tairan He, and Guanya Shi. Learning gentle humanoid locomotion and end-effector stabilization control. *arXiv preprint arXiv:2505.24198*, 2025.
- [9] Yuntao Ma, Farbod Farshidian, Takahiro Miki, Joonho Lee, and Marco Hutter. Combining learning-based locomotion policy with model-based manipulation for legged mobile manipulators. *IEEE Robotics and Automation Letters*, 7(2):2377–2384, 2022.
- [10] Yuanhang Zhang, Tianhai Liang, Zhenyang Chen, Yanjie Ze, and Huazhe Xu. Catch it! learning to catch in flight with mobile dexterous hands. In *2025 IEEE International Conference on Robotics and Automation (ICRA)*, pages 14385–14391, 2025.
- [11] Zipeng Fu, Xuxin Cheng, and Deepak Pathak. Deep whole-body control: Learning a unified policy for manipulation and locomotion. In Karen Liu, Dana Kulic, and Jeff Ichniowski, editors, *Proceedings of The 6th Conference on Robot Learning*, volume 205 of *Proceedings of Machine Learning Research*, pages 138–149. PMLR, 14–18 Dec 2023.
- [12] Aravind Elanjimattathil Vijayan, Andrei Cramariuc, Mattia Risiglione, Christian Gehring, and Marco Hutter. Multi-critic learning for whole-body end-effector twist tracking. In Joseph Lim, Shuran Song, and Hae-Won Park, editors, *Proceedings of The 9th Conference on Robot Learning*, volume 305 of *Proceedings of Machine Learning Research*, pages 1470–1485. PMLR, 27–30 Sep 2025.
- [13] Dianyong Hou, Chengrui Zhu, Zhen Zhang, Zhibin Li, Chuang Guo, and Yong Liu. Efficient learning of a unified policy for whole-body manipulation and locomotion skills. *arXiv preprint arXiv:2507.04229*, 2025.
- [14] Zifan Wang, Yufei Jia, Lu Shi, Haoyu Wang, Haizhou Zhao, Xueyang Li, Jinni Zhou, Jun Ma, and Guyue Zhou. Arm-constrained curriculum learning for locomotion-manipulation of a wheel-legged robot. In *2024 IEEE/RSJ International Conference on Intelligent Robots and Systems (IROS)*, pages 10770–10776. IEEE, 2024.
- [15] Huy Ha, Yihuai Gao, Zipeng Fu, Jie Tan, and Shuran Song. Umi on legs: Making manipulation policies mobile with manipulation-centric whole-body controllers. *arXiv preprint arXiv:2407.10353*, 2024.
- [16] Yuntao Ma, Yang Liu, Kaixian Qu, and Marco Hutter. Learning accurate whole-body throwing with high-frequency residual policy and pullback tube acceleration. *arXiv preprint arXiv:2506.16986*, 2025.
- [17] Fan Yang, Zhiwei Shi, Sixian Ye, Jiazhong Qian, Wenjie Wang, and Dong Xuan. Varsm: Versatile autonomous racquet sports machine. In *2022 ACM/IEEE 13th International Conference on Cyber-Physical Systems (CPS'22)*, pages 1–10. ACM, 2022.

- tional Conference on Cyber-Physical Systems (ICCPs)*, pages 203–214, 2022.
- [18] Zhongyu Li, Xue Bin Peng, Pieter Abbeel, Sergey Levine, Glen Berseth, and Koushil Sreenath. Reinforcement learning for versatile, dynamic, and robust bipedal locomotion control. *The International Journal of Robotics Research*, 44(5):840–888, 2025.
 - [19] Lerrel Pinto, Marcin Andrychowicz, Peter Welinder, Wojciech Zaremba, and Pieter Abbeel. Asymmetric actor critic for image-based robot learning. *arXiv preprint arXiv:1710.06542*, 2017.
 - [20] John Schulman, Filip Wolski, Prafulla Dhariwal, Alec Radford, and Oleg Klimov. Proximal policy optimization algorithms. *arXiv preprint arXiv:1707.06347*, 2017.
 - [21] Viktor Makoviychuk, Lukasz Wawrzyniak, Yunrong Guo, Michelle Lu, Kier Storey, Miles Macklin, David Hoeller, Nikita Rudin, Arthur Allshire, Ankur Handa, et al. Isaac gym: High performance gpu-based physics simulation for robot learning. *arXiv preprint arXiv:2108.10470*, 2021.
 - [22] Nikita Rudin, David Hoeller, Philipp Reist, and Marco Hutter. Learning to walk in minutes using massively parallel deep reinforcement learning. In *Conference on robot learning*, pages 91–100. PMLR, 2022.
 - [23] Caroline Cohen, Baptiste Darbois Texier, David Quéré, and Christophe Clanet. The physics of badminton. *New Journal of Physics*, 17(6):063001, 2015.
 - [24] Jemin Hwangbo, Joonho Lee, Alexey Dosovitskiy, Dario Bellicoso, Vassilios Tsounis, Vladlen Koltun, and Marco Hutter. Learning agile and dynamic motor skills for legged robots. *Science Robotics*, 4(26):eaau5872, 2019.
 - [25] Filip Bjelonic, Fabian Tischhauser, and Marco Hutter. Towards bridging the gap: Systematic sim-to-real transfer for diverse legged robots. *arXiv preprint arXiv:2509.06342*, 2025.

APPENDIX

A. System Parameters

Per-joint PD gains (Table I) list the proportional and derivative gains used by the 500 Hz joint-space PD controller for each controllable DoF in both simulation and deployment.

Actuator constants (Table II) summarize the four PhyArc actuator modules used on the robot, including physical size, reducer and gear ratio, nominal and no-load speeds (RPM), rated and peak torque (N·m), rated and peak power (W), and rotor inertia. These specifications are used to set torque/velocity limits, define dof properties, estimate power, and do safety checks in our experiments.

stiffness (N·m/rad)	damping (N·m·s/rad)	stiffness (N·m/rad)	damping (N·m·s/rad)
hip_pitch	100	hip_pitch	10
hip_roll	100	hip_roll	10
hip_yaw	100	hip_yaw	10
knee	50	knee	10
ankle_pitch	50	ankle_pitch	5
ankle_roll	5	ankle_roll	5
waist_yaw	100	waist_yaw	10
shoulder_pitch	50	shoulder_pitch	10
shoulder_roll	50	shoulder_roll	10
shoulder_yaw	5	shoulder_yaw	5
elbow_pitch	50	elbow_pitch	10

TABLE I: Per-joint PD gains

Actuator model (PhyArc series)	47	68	78	102
Size	$\varnothing 47 \times 68$	$\varnothing 68 \times 75$	$\varnothing 78 \times 79$	$\varnothing 102 \times 54.8$
Reducer type	Cycloid	Cycloid	Cycloid	Cycloid
Reduction ratio	25	25	25	25
Rated speed (RPM)	100	100	100	100
Rated torque (N·m)	3	28	40	60
No-load speed (RPM)	343.8	181.5	120	124.2
Rated power (W)	216	720	720	1080
Peak power (W)	864	4608	4608	5760
Peak torque (N·m)	12	96	136	244
Rotor inertia	0.00719	0.0339	0.0634	0.1734

TABLE II: Actuator constants

B. Training Details

Hyperparameters (Table III) define the PPO and training configuration used in our experiments. **Domain randomization and observation noise** (Table IV) specify the environment perturbations and sensor-noise settings applied during training. **Reward weights by stage** (Table V) records the curriculum's stage-wise weighting of r_{loco} , r_{hit} , and r_{global} . Together, these tables precisely describe the training setup and support reproducibility.

Hyperparameter	Setting
discount factor	0.99
GAE lambda	0.95
learning rate	adaptive
KLD target	0.01
clip param	0.2
control dt (s)	0.02
num. envs	4096
actor MLP size	(512, 256, 128)
critic MLP size	(512, 256, 128)
network activation	elu
optimizer	AdamW

TABLE III: Hyperparameter configuration

Domain random	Range	Noise	Range
friction range	[0.5, 1.0]	dof_pos	0.05
push interval	5	dof_vel	0.2
max push vel_xy	0.5	lin_vel	0.2
max push ang_vel	0.5	ang_vel	0.1
added base_com range	[-0.08, 0.08]	gravity	0.1
join_friction range	[0.01, 1.0]		
added inertia range	[0.01, 0.1]		

TABLE IV: Domain randomization and observation noise

TABLE V: Reward weights by stage

Stage	Category	Term	Weight
S1			
S1	r_{loco}	base_height	5
S1	r_{loco}	base_acc	1
S1	r_{loco}	base_ang_vel_xy	-10
S1	r_{loco}	base_orientation	-50
S1	r_{loco}	contact_no_vel	-10
S1	r_{loco}	feet_orientation	10
S1	r_{loco}	no_fly	2
S1	r_{loco}	feet_height	10
S1	r_{loco}	feet_distance	2
S1	r_{loco}	momentum_positive	5
S1	r_{loco}	air_time & land_time	-500
S1	r_{loco}	sym_contact_forces	1
S1	r_{loco}	sym_step	-5
S1	r_{loco}	face_the_net	8
S1	r_{loco}	target_approach	30
S1	r_{hit}	—	—
S1	r_{global}	action_rate	-0.8
S1	r_{global}	joint_position_limit	-30
S1	r_{global}	joint_velocity_limit	-0.1
S1	r_{global}	joint_torque_limit	-0.1
S1	r_{global}	dof_acc	-5×10^{-5}
S1	r_{global}	dof_vel	-1×10^{-3}
S1	r_{global}	dof_torque	-1×10^{-4}
S2			
S2	r_{loco}	base_height	5
S2	r_{loco}	base_acc	1
S2	r_{loco}	base_ang_vel_xy	-10
S2	r_{loco}	base_orientation	-50

Stage	Category	Term	Weight
S2	r_{loco}	contact_no_vel	-10
S2	r_{loco}	feet_orientation	10
S2	r_{loco}	no_fly	2
S2	r_{loco}	feet_height	10
S2	r_{loco}	feet_distance	2
S2	r_{loco}	momentum_positive	5
S2	r_{loco}	air_time & land_time	-500
S2	r_{loco}	sym_contact_forces	1
S2	r_{loco}	sym_step	-5
S2	r_{loco}	face_the_net	5
S2	r_{loco}	target_approach	15
S2	r_{hit}	r_{swing}	4000
S2	r_{hit}	$r_{y\text{-align}}$	5
S2	r_{hit}	r_{hold}	10
S2	r_{global}	action_rate	-0.8
S2	r_{global}	joint_position_limit	-30
S2	r_{global}	joint_velocity_limit	-0.1
S2	r_{global}	joint_torque_limit	-0.5
S2	r_{global}	dof_acc	-5×10^{-5}
S2	r_{global}	dof_vel	-1×10^{-3}
S2	r_{global}	dof_torque	-1×10^{-4}
S2	r_{global}	energy	-0.01
S2	r_{global}	collision	-10
S3			
S3	r_{loco}	base_height	5
S3	r_{loco}	base_acc	1
S3	r_{loco}	base_ang_vel_xy	-10
S3	r_{loco}	base_orientation	-50
S3	r_{loco}	contact_no_vel	-10
S3	r_{loco}	feet_orientation	10
S3	r_{loco}	momentum_positive	5
S3	r_{loco}	air_time & land_time	-500
S3	r_{loco}	face_the_net	8
S3	r_{hit}	r_{swing}	4000
S3	r_{hit}	$r_{y\text{-align}}$	5
S3	r_{hit}	r_{hold}	10
S3	r_{global}	action_rate	-0.8
S3	r_{global}	joint_position_limit	-30
S3	r_{global}	joint_velocity_limit	-0.1
S3	r_{global}	joint_torque_limit	-0.5
S3	r_{global}	dof_acc	-5×10^{-5}
S3	r_{global}	dof_vel	-1×10^{-3}
S3	r_{global}	dof_torque	-1×10^{-4}
S3	r_{global}	energy	-0.01
S3	r_{global}	collision	-10

$$\begin{cases} p_{x,t_0} \sim U(5, 8) \\ p_{y,t_0} \sim U(-2, 2) \\ p_{z,t_0} \sim U(-0.5, 2.5) \\ v_{x,t_0} \sim U(-25, -13) \\ v_{y,t_0} \sim U(-3, 3) \\ v_{z,t_0} \sim U(9, 18) \end{cases} \quad (8)$$

This study develops a shuttlecock trajectory generator based on aerodynamic principles, employing numerical integration to simulate flight trajectories and filtering them according to predefined hitting criteria for robot training purposes, as illustrated in Fig. 8. The specific characteristics of a single trajectory are examined in Fig. 9.

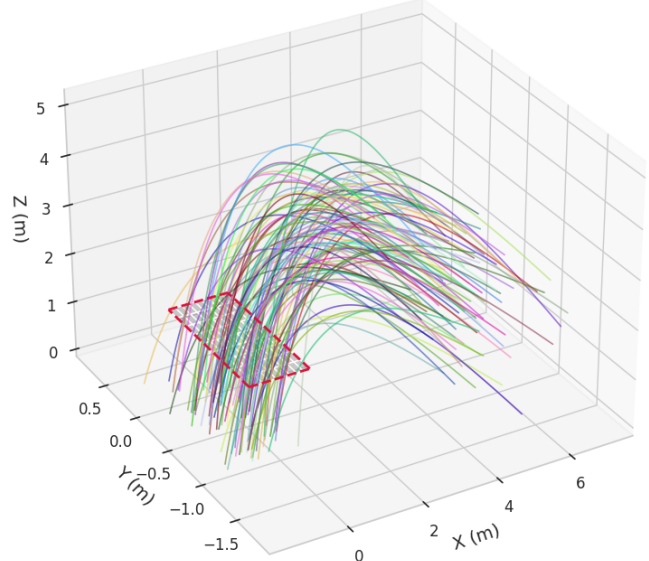


Fig. 8: **Trajectory generation.** Shuttlecock trajectories are filtered to ensure interception points within the region $x \in [-0.8, 0.8] \text{ m}$, $y \in [-1, 0.2] \text{ m}$ and $z \in [1.5, 1.6] \text{ m}$ for robot training.

C. Supplementary Explanation for Model-based Hitting Target Generation

During trajectory generation, we employed a fixed time step for each trajectory and updated the shuttlecock's position and velocity through numerical integration. The initial positions and velocities were randomly generated within specified ranges to ensure diversity in the training data, with detailed settings in (8) [6]:

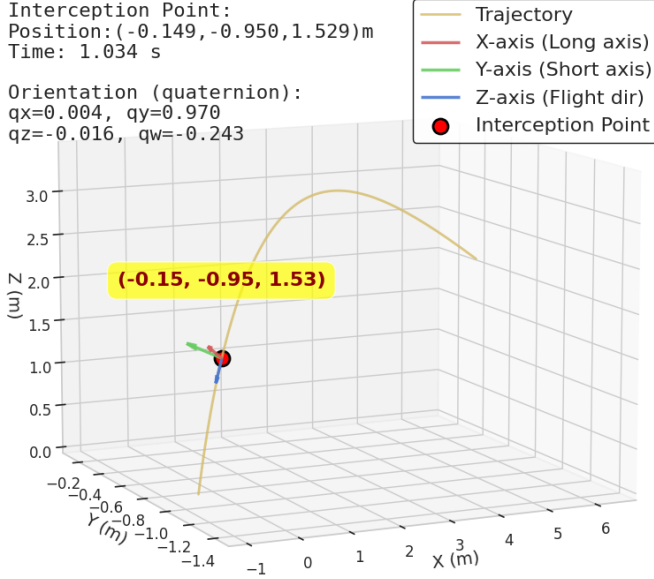


Fig. 9: **Individual trajectory analysis.** An example of sampled shuttle flight trajectory (gold) with the selected interception point (red). Corresponding target frame at the intercept is drawn, where z is the incoming-flight direction. The annotation reports the intercept position, orientation and time-to-intercept.

We generated 2 million trajectories, from which 19,685 met the criteria and were selected for robot training. The majority of these trajectories reached the hitting zone within a time interval of [0.8, 1.4] seconds, as shown in Fig. 10.

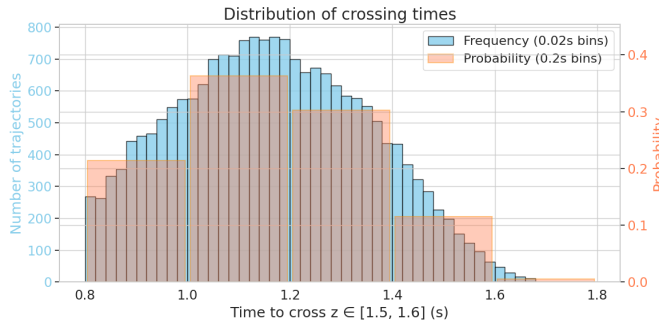


Fig. 10: **Training trajectory statistics.** Distribution of the shuttlecock interception time.

D. Repeatability Accuracy of Swing

During the real-world Virtual-Target Swinging test, we assessed repeatability precision by commanding a single fixed interception target and executing 20 independent swings. The racket center was tracked in real time using a motion-capture system. At the designated hit instant, positional error was defined as the distance between the captured racket-center coordinate and the target position. The resulting 3D trajectories of the racket center across the 20 trials are presented in Fig. 11,

while Fig. 12 visualizes the distance between the racket center and the target position over time.

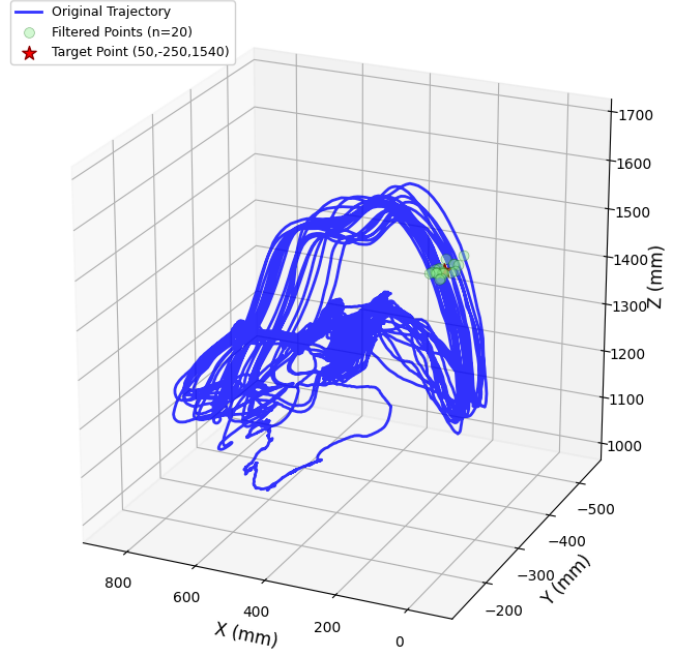


Fig. 11: **Trajectory of the racket center.** For a designated hitting position at (50, -250, 1540) mm, the robot executed 20 swinging motions. The green spheres represent the positions of the racket center as it passed through the $z = 1540$ mm plane during each swing.

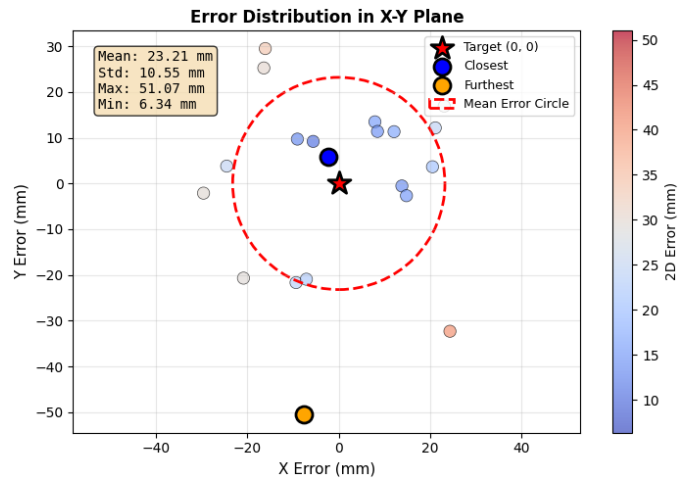


Fig. 12: **Swing Error Analysis.** Over 20 repeated swings, the mean Euclidean distance error was measured at 23.21 mm, with a standard deviation of 10.55 mm. The maximum and minimum errors recorded were 51.07 mm and 6.34 mm, respectively.